Magnetic properties of epitaxial Heusler alloy $(Co_{2/3}Fe_{1/3})_{3+x}Si_{1-x}$/GaAs(001) hybrid structures

2006 J. Phys.: Condens. Matter 18 6101

(http://iopscience.iop.org/0953-8984/18/26/028)

INSTITUTE OF PHYSICS PUBLISHING JOURNAL OF PHYSICS: CONDENSED MATTER

J. Phys.: Condens. Matter **18** (2006) 6101–6108 doi:10.1088/0953-8984/18/26/028

Magnetic properties of epitaxial Heusler alloy $(Co_{2/3}Fe_{1/3})_{3+x}Si_{1-x}$/GaAs(001) hybrid structures

M Hashimoto, J Herfort, H-P Schönherr and K H Ploog

Paul-Drude-Institut für Festkörperelektronik, Hausvogteiplatz 5–7, 10117 Berlin, Germany

E-mail: hashimoto@pdi-berlin.de

Received 24 March 2006, in final form 28 April 2006
Published 19 June 2006
Online at stacks.iop.org/JPhysCM/18/6101

Abstract

The magnetic properties of full Heusler alloy $(Co_{2/3}Fe_{1/3})_{3+x}Si_{1-x}$/GaAs(001) hybrid structures grown by molecular beam epitaxy have been investigated. The magnetic moment, the coercive field and the in-plane magnetic anisotropy of $(Co_{2/3}Fe_{1/3})_{3+x}Si_{1-x}$ films with various Si compositions ($-0.46 \leqslant x \leqslant 1$) are discussed. The increase in amount of Si results in a significant reduction in the cubic magnetocrystalline anisotropy constant $|K_1^{\mathrm{eff}}|$. K_1^{eff} changes sign and saturates near the stoichiometric composition of Co_2FeSi and the easy axis of the cubic component changes from the $\langle 110 \rangle$ direction to the $\langle 100 \rangle$ direction accordingly. However, due to the presence of a dominating uniaxial magnetic anisotropy component, the easy axis of magnetization in total is shifted to the [110] direction. The saturation magnetization of stoichiometric Co_2FeSi films turned out to be 1250 ± 120 emu cm^{-3}, being equivalent to 6.1 ± 0.57 (μ_B/formula unit (fu)). The relatively close value of magnetic moment to the theoretically expected integer value (6 μ_B) suggests that Co_2FeSi films could be half-metallic ferromagnets.

(Some figures in this article are in colour only in the electronic version)

1. Introduction

Half-metallic ferromagnets (HMFs), which have 100% spin-polarized carriers at the Fermi level, are promising candidates for spintronics devices, e.g. magnetic tunnelling junction and spin injection device. Potential HMFs include some diluted magnetic semiconductors, oxides and Heusler alloys. Heusler alloys are especially attractive because of their high Curie temperature, close lattice matching with semiconductors and theoretically predicted half-metallicity [1]. Some Heusler alloys, e.g. NiMnSb, Co_2MnSi, and Co_2MnGe, are predicted to be half-metallic by theoretical studies [2–5]. Moreover, recently we have clarified that Heusler alloy/semiconductor (SC) hybrid structures have a more thermally stable interface

than conventional elemental ferromagnets (FM)/SC [6, 7]. Therefore, Heusler alloy/SC hybrid structures are much more suitable for device-processing steps after epitaxial growth.

Co_2FeSi is a full Heusler alloy with a cubic $L2_1$ crystal structure consisting of four interpenetrating fcc sublattices [8]. The lattice constant of bulk Co_2FeSi is 5.658 Å [9], being closely lattice matched to GaAs ($a_{GaAs} = 5.653$ Å). The lattice mismatch is as small as 0.08%. Bulk Co_2FeSi with a large magnetic moment (5.91 μ_B at 10.2 K) is ferromagnetic up to more than 980 K [9]; these are among the highest Curie temperatures and magnetic moments of the reported Heusler alloys. According to electronic band structure calculations based on the local density approximation (LDA), Co_2FeSi is located at a position slightly deviating from the Slater–Pauling curve which half-metallic Heusler alloys are expected to obey [5]. On the other hand, recent calculations based on LDA + U, which take into account the electron correlation effect, have revealed that Co_2FeSi can have an integer magnetic moment (6 μ_B/formula unit (fu)), suggesting that it should be a HMF [10]. These characteristics make this material promising for applications in spintronic devices.

The $L2_1$ structure can also be considered as a combination of two binary B2 alloys, i.e. CoFe and CoSi in the case of Co_2FeSi [8]. Since binary CoFe does crystallize in the B2 structure when it is ordered, it is possible to tune the composition continuously from the binary CoFe to the Heusler alloy Co_2FeSi by changing the Si composition. This enables a systematic study of the transition of its magnetic properties between the two different classes of alloys in the present system. In this report, we study the magnetic properties of full Heusler alloy $(Co_{2/3}Fe_{1/3})_{3+x}Si_{1-x}$ films ($-0.46 \leqslant x \leqslant 1$) having various Si compositions including binary $Co_{0.66}Fe_{0.34}$ grown by molecular beam epitaxy (MBE) on GaAs(001) substrates. The impact of Si incorporation on the magnetic moment, coercive field and in-plane magnetic anisotropy of $(Co_{2/3}Fe_{1/3})_{3+x}Si_{1-x}$ is described.

2. Sample preparation

In preparation of the Co_2FeSi, the growth conditions of the binary alloy $Co_{0.66}Fe_{0.34}$ (bcc structure) were optimized. The composition of $Co_{0.66}Fe_{0.34}$ layers was determined by comparing their lattice constant with literature data [11], taking into account the tetragonal distortion of the layers as confirmed by reciprocal space mappings around the (113) and (224) reflections (not shown here). To estimate the unstrained lattice constant of the films the elastic constants of CoFe [12] have been used. Then Si was added and incorporated to obtain ternary $(Co_{2/3}Fe_{1/3})_{3+x}Si_{1-x}$, while the Fe and Co fluxes were kept constant at the determined amounts.

Before the growth of the $(Co_{2/3}Fe_{1/3})_{3+x}Si_{1-x}$ layers, 100 nm-thick GaAs buffer layers were grown in the III–V growth chamber using standard GaAs growth conditions. As-terminated c(4 × 4) reconstructed GaAs(001) surfaces were prepared by cooling the samples down to 420 °C under As_4 pressure to prevent the formation of macroscopic defects on the surface similar to our studies on Fe/GaAs(001) [13]. The samples were then transferred to the As-free metal deposition chamber under UHV at a base pressure of 5×10^{-10} Torr. The growth temperature T_G for the $Co_{0.66}Fe_{0.34}$ and $(Co_{2/3}Fe_{1/3})_{3+x}Si_{1-x}$ layers was kept at 100 °C due to the requirement of low T_G to avoid the interfacial reaction in CoFe/GaAs growth. We confirmed that the Co_2FeSi/GaAs interface is thermally robust up to $T_G = 200$ °C [7]. A low growth rate of about 0.1 nm min^{-1} was chosen in order to avoid the degradation of the crystal quality at this low growth temperature. The Si cell temperature T_{Si}, and hence the composition of the films, was varied from 1280 to 1335 °C. Correspondingly the perpendicular lattice mismatch between the layer and the substrate $(\Delta a/a)_\perp$ varied linearly from 0.76% ($T_{Si} = 1280$ °C) to −0.47% ($T_{Si} = 1325$ °C) [14]. Further elevation of T_{Si} resulted in a

substantial reduction of the $Co_2FeSi(004)$ reflection peak in the ω–2θ curve at $T_{Si} = 1335\,^{\circ}C$ due to crystal degradation. From a comparison of a_{Co_2FeSi} with that of the bulk value, the stoichiometric film was determined to have a tetragonal distortion of $(\Delta a/a)_{\perp} = 0.14\%$ [14]. Then the Si composition x of $(Co_{2/3}Fe_{1/3})_{3+x}Si_{1-x}$ was estimated, by interpolation from the lattice constants, to be in the range $-0.46 \leqslant x \leqslant 1$. In this notation, $x = -3$, 0 and 1 correspond to pure Si, stoichiometric Co_2FeSi and $Co_{0.66}Fe_{0.34}$, respectively. The thickness of the layers determined by high-resolution x-ray diffraction (HRXRD) and x-ray reflectivity (XRR) measurements varies in the range from 17 to 23 nm in accordance with the constant growth time of 180 min and the increase of T_{Si}. An atomically abrupt interface was confirmed from the observation of interference fringes in the HRXRD ω–2θ curves and by transmission electron microscopy for the film grown at 100 °C [7]. The long-range atomic ordering, namely the formation of the Heusler-type $L2_1$ structure even at this low T_G for samples around stoichiometric Co_2FeSi, is confirmed by the presence of the (113) and (002) superlattice reflection [15]. More details of the growth and structural characterizations are described elsewhere [14, 15].

3. Results and discussions

The magnetic properties of the $(Co_{2/3}Fe_{1/3})_{3+x}Si_{1-x}$ films were investigated using superconducting quantum interference device (SQUID) magnetometry. All the measurements were performed at room temperature and the external magnetic field was applied along three different in-plane crystallographic axes, [110], [1$\bar{1}$0] and [100]. After subtracting the diamagnetic contribution of the GaAs substrate, the magnetization was normalized to the saturation magnetization M_s. The films were not capped. However, we consider its influence on the magnetic moment to be much smaller than that from the uncertainty of volume estimation. All the examined $(Co_{2/3}Fe_{1/3})_{3+x}Si_{1-x}$ films are ferromagnetic at room temperature with the easy axis along the [110] direction. The obtained magnetization curves of the $(Co_{2/3}Fe_{1/3})_{3+x}Si_{1-x}$ films were categorized into three types: (i) $Co_{0.66}Fe_{0.34}$ ($x = 1$) where a so-called split loop was observed along the [1$\bar{1}$0] direction; (ii) $(Co_{2/3}Fe_{1/3})_{3+x}Si_{1-x}$ with $-0.46 \leqslant x \leqslant 0.46$, where an uniaxial magnetic anisotropy (UMA) dominates; and (iii) $(Co_{2/3}Fe_{1/3})_{3+x}Si_{1-x}$ with $x < -0.46$, where a degradation of the crystalline quality occurred. The normalized magnetization curves of each type are displayed in figure 1 together with the magnetization curves along the easy axis direction in an expanded scale in the right panel.

The magnetization curves of $Co_{0.66}Fe_{0.34}$ show a square-shaped hysteresis loop with a relatively large H_c of 20 Oe along the easy axis, a split loop along the [1$\bar{1}$0] direction, and a strong hard axis with a saturation field H_{sat} of about 1000 Oe along the [100] direction (figures 1(d) and (h)). The incorporation of Si into $Co_{0.66}Fe_{0.34}$ induces several changes in the magnetization curves. We see a disappearance of the split loop, reductions of H_c and H_{sat} along the [100] direction as the composition approaches stoichiometry in figures 1(c), (g), (b) and (f). The magnetization curves of stoichiometric Co_2FeSi shows an easy axis [110], a reversible hard axis [1$\bar{1}$0] and an intermediate axis [100] as can be seen in figures 1(b) and (f). The magnetization curve along the [110] direction shows a square-shaped hysteresis loop with a significantly reduced coercive field H_c of 4.5 Oe, indicating an excellent crystalline quality. The reversible hard axis along the [1$\bar{1}$0] direction indicates the presence of an in-plane UMA component. This is typical in cubic FM grown on zinc-blende SC systems [16–19] and is attributed to an anisotropic bonding at the FM/SC interface [20]. The saturation field H_{sat} along the $\langle 100 \rangle$ direction is significantly reduced to $H_{sat} \approx 200$ Oe, which can be associated with a reduction of the cubic magnetic anisotropy component, such that UMA becomes the

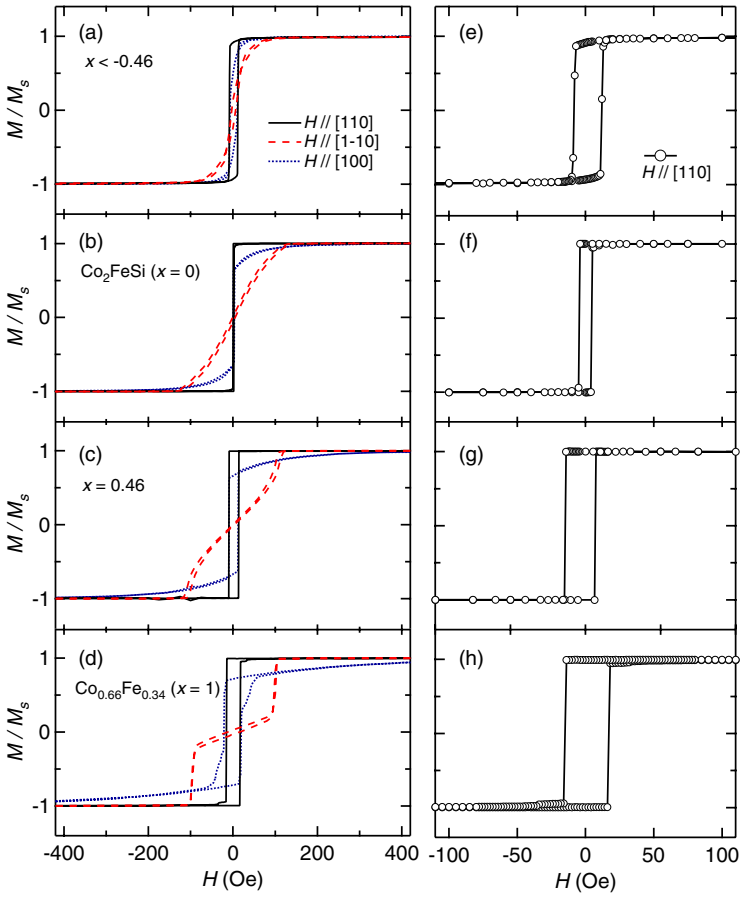

Figure 1. Normalized magnetization curves of: (a), (e) $(Co_{2/3}Fe_{1/3})_{3+x}Si_{1-x}$ with $x < -0.46$; (b), (f) stoichiometric Co_2FeSi ($x = 0$); (c), (g) $(Co_{2/3}Fe_{1/3})_{3+x}Si_{1-x}$ with $x = 0.46$; and (d), (h) $Co_{0.66}Fe_{0.34}$ ($x = 1$). All curves were taken at room temperature. The external magnetic field was applied along three different crystallographic axes, [110], [1$\bar{1}$0] and [100]. The right panel (e)–(g) shows the magnetization curves along the easy axis in an expanded scale. The diamagnetic contribution of the substrate has been subtracted.

dominating component in its in-plane magnetic anisotropy. The excessive incorporation of Si results in a further modification of the magnetization curves, as can be seen in figures 1(a) and (e). The magnetization curve becomes a rounder-shaped square with an increased H_c due to the crystal degradation. In addition, the in-plane UMA is further reduced.

M_s and H_c of the $(Co_{2/3}Fe_{1/3})_{3+x}Si_{1-x}$ films are plotted as a function of Si composition x in figure 2. H_c is along the [110] direction. M_s decreases almost linearly with increasing Si composition. The rather large scatter of the data is due to the uncertainty in determining the exact volume of the $(Co_{2/3}Fe_{1/3})_{3+x}Si_{1-x}$ layers. M_s of $Co_{0.66}Fe_{0.34}$ (1800 ± 74 emu cm^{-3} $\simeq$ 210 ± 9 emu g^{-1}) is comparable to the literature data of 1710 emu cm^{-3} [19] and 219.94 and 209.96 emu g^{-1} for bulk $Co_{0.6}Fe_{0.4}$ and $Co_{0.7}Fe_{0.3}$, respectively, in [21]. The M_s of the stoichiometric Co_2FeSi film amounts to 1250 ± 120 emu cm^{-3}, being equivalent to 6.1 ± 0.57 (μ_B/fu). Although the error is rather large, the value is relatively close to the theoretically expected integer value of 6 (μ_B/fu), suggesting that thin Co_2FeSi films could be

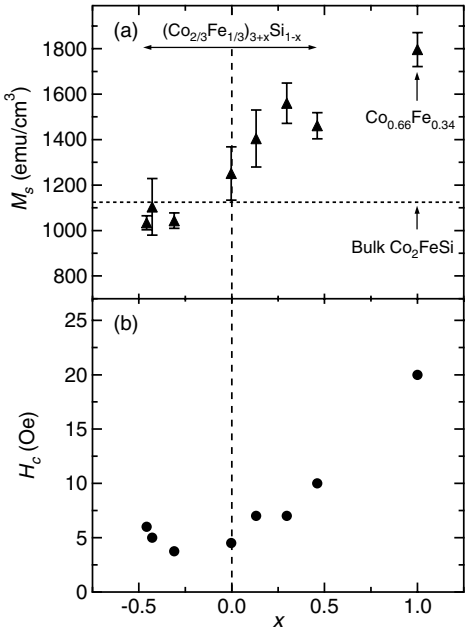

Figure 2. (a) Saturation magnetization M_s and (b) coercive field H_c along the [110] direction as a function of the Si content x for $Co_{0.66}Fe_{0.34}$ and $(Co_{2/3}Fe_{1/3})_{3+x}Si_{1-x}$. The dotted and dashed lines are M_s of bulk Co_2FeSi [9] and the stoichiometric composition of Co_2FeSi determined by HRXRD, respectively.

a HMF. The relatively large M_s of the stoichiometric film compared to that of bulk Co_2FeSi (1124 emu cm^{-3} at 295 K) may be due to a rather high degree of disorder (10–16%) in the bulk Co_2FeSi [9]. However, although the $L2_1$ structure was revealed for the films studied, the determination of the degree of ordering is currently under way. M_s remains nearly constant upon elevation of T_G up to 250 °C and gradually decreases above 250 °C, most likely due to the formation of a magnetically modified layer at the interface [7]. H_c decreases from the value of $Co_{0.66}Fe_{0.34}$ with increasing Si composition as shown in figure 2(b). H_c shows a minimum region in $-0.31 \leqslant x \leqslant 0$. Note that generally structural degradation of the layer and interface will increase H_c. Hence the minimum region corresponds to the region where an excellent crystal quality is maintained around the stoichiometric composition.

In order to explain the changes in the magnetization curves, the in-plane magnetic anisotropy of $(Co_{2/3}Fe_{1/3})_{3+x}Si_{1-x}$ was investigated by assuming a free energy density consisting of a cubic magnetocrystalline anisotropy term and an UMA term:

$$\varepsilon(\phi) = -\tfrac{1}{4}K_1^{\text{eff}}\sin^2(2\phi) + K_u^{\text{eff}}\sin^2(\phi) - HM_s\cos(\phi - \alpha), \tag{1}$$

where α is the angle between the external field and the [110] direction and ϕ is the angle between magnetization and the [110] direction [19]. Assuming a coherent rotation as a magnetization reversal process, by minimizing $\varepsilon(\phi)$, we obtain the relation between magnetic field H and magnetization M:

$$H(m) = 2K_1^{\text{eff}}(2m^3 - m)/M_s + 2K_u^{\text{eff}}m/M_s \tag{2}$$

where $m = \sin(\phi)$ is the normalized magnetization component [19]. Fitting the magnetization curves along the $[1\bar{1}0]$ direction with this expression, two effective anisotropy constants, K_1^{eff} and K_u^{eff}, were obtained. For the magnetization curves which show a discontinuous split loop,

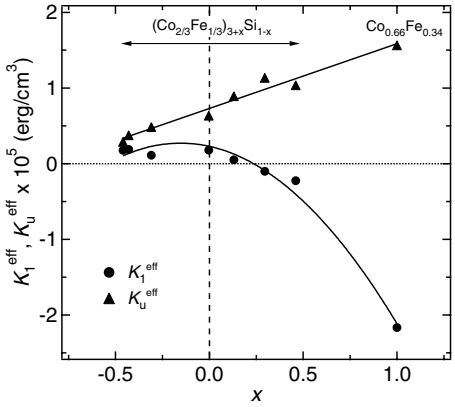

Figure 3. K_1^{eff} and K_u^{eff} of $Co_{0.66}Fe_{0.34}$ and $(Co_{2/3}Fe_{1/3})_{3+x}Si_{1-x}$ as a function of the Si content x. The dashed line is the stoichiometric composition determined by HRXRD and the solid lines are guides for the eye.

as in the case of $Co_{0.66}Fe_{0.34}$ with $H \parallel [1\bar{1}0]$, the anisotropy constants can be obtained using the following expressions derived from the same model (equation (1)),

$$K_1^{\mathrm{eff}} = \frac{1}{2}\frac{M_s(-1 + H_s s)}{(H_s^3 s^3 + H_s^2 s^2 + H_s s + 1)s}, \tag{3}$$

$$K_u^{\mathrm{eff}} = \frac{1}{2}\frac{M_s H_s (H_s^2 s^2 + H_s s + 2)}{H_s^3 s^3 + H_s^2 s^2 + H_s s + 1} \tag{4}$$

where s and H_s are the slope near $H = 0$ and the split field where the discontinuity takes place, respectively [19]. All the experimental magnetization curves were fitted well with this model, indicating that the magnetization reversal process takes place by a coherent rotation of magnetization as a single domain. In order to check the validity of the fitting, we performed simulations of the magnetization curves along the other two directions with the Stoner–Wohlfarth model using the obtained magnetic anisotropy constants, K_1^{eff} and K_u^{eff}. We obtained an excellent agreement between the simulated and experimental results for the reversible parts of the magnetization curves, suggesting the validity of the single-domain coherent-rotation model as well as the obtained magnetic anisotropy constants. On the other hand, the irreversible parts, i.e. H_c, were not reproduced since the Stoner–Wohlfarth model does not take into account the micro-magnetic structure of the layer [22].

K_1^{eff} and K_u^{eff} of the $(Co_{2/3}Fe_{1/3})_{3+x}Si_{1-x}$ films are plotted as a function of x in figure 3. As can be seen in the figure, K_u^{eff} linearly decreases with increasing Si content. This is partly due to the fact that K_u^{eff} is inversely proportional to the film thickness since K_u^{eff} is a pure interface-related term [15]. However, as far as the proportion of the interface contribution only is concerned, the expected decrease of K_u^{eff} corresponding to the thickness ranging from 17 to 23 nm is only $\Delta K_u^{\mathrm{eff}} = (-1.1 \pm 0.1) \times 10^4$ erg cm^{-3}. The value was estimated using the interface contribution constant of UMA, $K_u^{\mathrm{int}} = (7.2 \pm 0.9) \times 10^{-2}$ erg cm^{-2} [15]. This is almost one order of magnitude smaller than the actual decrease of $\Delta K_u^{\mathrm{eff}} = -7.4 \times 10^4$ erg cm^{-3}. Therefore, the reduction of K_u^{eff} cannot be attributed to the decrease of the interface contribution with increasing d but to a modification of the Co_2FeSi/GaAs interface itself. Most likely it reflects the modification of the bonding configuration at the interface by the incorporation of Si. On the other hand, $|K_1^{\mathrm{eff}}|$ decreases with increasing Si content. K_1^{eff} changes the sign and subsequently saturates near the stoichiometric composition of Co_2FeSi. The change of the

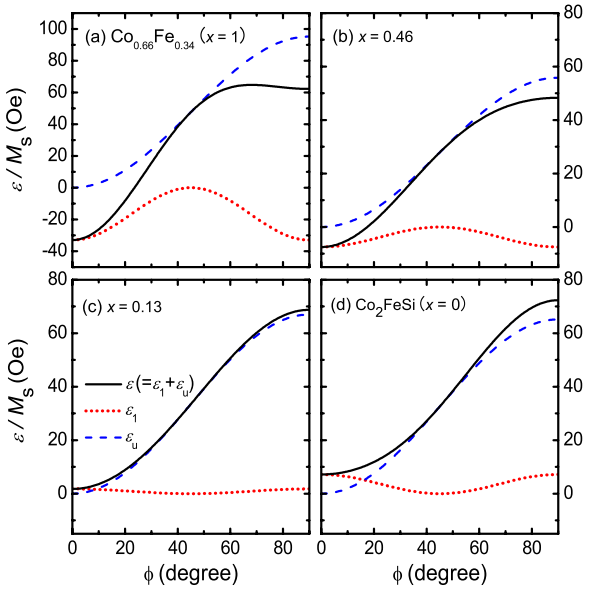

Figure 4. Free energy density $\varepsilon(\phi)$ calculated by using the fitted anisotropy constants K_1^{eff} and K_u^{eff} for (a) $Co_{0.66}Fe_{0.34}$ and ((b)–(d)) $(Co_{2/3}Fe_{1/3})_{3+x}Si_{1-x}$ having different Si contents. Total free energy density (black line), contribution from the magnetocrystalline anisotropy ε_1 (red dotted line) and from the uniaxial anisotropy ε_u (blue dashed line) is shown.

sign and the saturation of K_1^{eff} most likely corresponds to the change of the crystal structure from the bcc structure of $Co_{0.66}Fe_{0.34}$ into the $L2_1$ structure as evidenced by the appearance of the superlattice reflections (002) and (113) in the Co_2FeSi films [15]. As a result, the UMA is dominant near the stoichiometric composition, as already shown in the magnetization curves (figure 1(b)). The anisotropy constants of the Co_2FeSi ($d = 18.5$ nm) and $Co_{0.66}Fe_{0.34}$ (17.4 nm) films turned out to be $K_1^{\text{eff}} = 1.8 \times 10^4$ erg cm^{-3}, $K_u^{\text{eff}} = 6.3 \times 10^4$ erg cm^{-3} and $K_1^{\text{eff}} = -2.2 \times 10^5$ erg cm^{-3}, $K_u^{\text{eff}} = 1.6 \times 10^5$ erg cm^{-3}, respectively. The K_1^{eff} of $Co_{0.66}Fe_{0.34}$ is comparable to the literature value (-2.85×10^5 erg cm^{-3} [19]), while K_u^{eff} is one order of magnitude larger than that of the literature (1.5×10^4 erg cm^{-3} [19]). We assume that the comparatively large K_u^{eff} value, despite the rather large thickness of the $(Co_{2/3}Fe_{1/3})_{3+x}Si_{1-x}$ films, can be ascribed to the excellent interface perfection of the hybrid structure caused by the low growth temperature as well as the low growth rate.

In order to obtain further insights into the in-plane magnetic anisotropy depending on the Si composition and its relevance to the magnetization reversal process, we calculated the angle dependence of the free energy density $\varepsilon(\phi)$ with equation (1) using the obtained anisotropy constants. Figure 4 shows the angle dependence of the free energy density together with the UMA and cubic magnetocrystalline anisotropy components of (a) the $Co_{0.66}Fe_{0.34}$ film and (b)–(d) several $(Co_{2/3}Fe_{1/3})_{3+x}Si_{1-x}$ films having different Si contents. In the case of $Co_{0.66}Fe_{0.34}$, a relatively large K_u^{eff} component shares the common easy axis with the cubic magnetocrystalline anisotropy component at $\phi = 0°$, in the [110] direction. As a result, the total $\varepsilon(\phi)$ has a local minimum at $\phi = 90°$, in the $[1\bar{1}0]$ direction. This condition allows the magnetization to jump from near the [110] direction to the $[1\bar{1}0]$ direction and vice versa at H_s, resulting in the split loop [23]. As the formation of the $L2_1$ structure develops, the cubic magnetocrystalline anisotropy becomes weakened. It changes the sign at $x = 0.13$ (figure 4(c)), and accordingly the position of the minima of the cubic magnetocrystalline component rotates

by 45°. Therefore, the inherent easy axis of Co_2FeSi is along the ⟨100⟩ direction, although it appears to be along the [110] direction. Namely, due to the presence of the relatively strong UMA, which has a conflicting easy axis with the cubic magnetocrystalline one, the easy axis is in total shifted to the [110] direction.

4. Conclusion

We have studied the magnetic properties of epitaxial Heusler alloy $(Co_{2/3}Fe_{1/3})_{3+x}Si_{1-x}$/GaAs(001) hybrid structures. The magnetic moment, coercive field and in-plane magnetic anisotropy of $(Co_{2/3}Fe_{1/3})_{3+x}Si_{1-x}$ with various Si contents ($-0.46 \leqslant x \leqslant 1$) were described. Incorporation of Si into $Co_{0.66}Fe_{0.34}$ results in a significant reduction of the cubic magnetocrystalline anisotropy constant $|K_1^{\mathrm{eff}}|$. K_1^{eff} changes its sign and saturates near the stoichiometric composition. Due to the dominating uniaxial magnetic anisotropy component, the easy axis of magnetization in total is shifted to the [110] direction. The magnetic moment of the stoichiometric Co_2FeSi films is relatively close to the theoretically expected integer value of 6 (μ_B/fu), suggesting that Co_2FeSi could be a half-metallic ferromagnet. These results make this material promising for spintronics applications.

Acknowledgments

This work was partly supported by the German BMBF under the research programme NanoQUIT (contract no 01BM463). The authors would like to thank L Pérez for useful discussions and for a careful reading of the manuscript.

References

[1] Palmstrøm C 2003 *Mater. Res. Soc. Bull.* **28** 725
[2] de Groot R, Mueller F, van Engen P and Buschow K 1983 *Phys. Rev. Lett.* **50** 2024
[3] Fujii S, Sugimura S, Ishida S and Asano S 1990 *J. Phys.: Condens. Matter* **2** 8583
[4] Ishida S, Fujii S, Kashiwagi S and Asano S 1995 *J. Phys. Soc. Japan* **654** 2152
[5] Galanakis I, Dederichs P H and Papanikolau N 2002 *Phys. Rev.* B **66** 174429
[6] Herfort J, Schönherr H-P and Ploog K H 2003 *Appl. Phys. Lett.* **83** 3912
Herfort J, Jenichen B, Kaganer V, Trampert A, Schönherr H-P and Ploog K H 2006 *Physica* E **32** 371
[7] Hashimoto M, Herfort J, Trampert A, Schönherr H-P and Ploog K H 2006 *J. Vac. Sci. Technol.* B at press
[8] Webster P J and Ziebeck K R A 1988 *Landolt–Börnstein New Series III/19c* (Berlin: Springer) p 75
[9] Niculescu V, Budnick J I, Hines W A, Raj K, Pickart S and Skalski S 1979 *Phys. Rev.* B **19** 452
[10] Wurmehl S, Fecher G H, Kandpal H C, Ksenofontov V, Felser C, Lin H-J and Morais J 2005 *Phys. Rev.* B **72** 184434
[11] Nishizawa T and Ishida K 1984 *Bull. Alloy Phase Diagrams* **5** 250
[12] Hearmon R F S 1979 *Landolt–Börnstein New Series III/11* (Berlin: Springer) p 12
[13] Schönherr H-P, Nötzel R, Ma W and Ploog K H 2001 *J. Appl. Phys.* **89** 169
[14] Hashimoto M, Herfort J, Schönherr H-P and Ploog K H 2005 *Appl. Phys. Lett.* **87** 102506
[15] Hashimoto M, Herfort J, Schönherr H-P and Ploog K H 2005 *J. Appl. Phys.* **98** 104902
[16] Krebs J J, Jonker B T and Prinz G A 1987 *J. Appl. Phys.* **61** 2596
[17] Kneedler E M, Jonker B T, Thibado P M, Wagner R J, Shanabrook B V and Whitman L J 1997 *Phys. Rev.* B **56** 8163
[18] Reiger E, Reinwald E, Garreau G, Ernst M, Zölfl M, Bensch F, Bauer S, Preis H and Bayreuther G 2000 *J. Appl. Phys.* **87** 5923
[19] Dumm M, Zölfl M, Moosbühler R, Brockmann M, Schmidt T and Bayreuther G 2000 *J. Appl. Phys.* **87** 5457
[20] Sjöstedt E, Nordström L, Gustavsson F and Eriksson O 2002 *Phys. Rev. Lett.* **89** 267203
[21] Bardos D I 1969 *J. Appl. Phys.* **40** 1371
[22] Daboo C, Hicken R J, Gu E, Gester M, Gray S J, Eley D E P, Ahmad E, Bland J A C, Ploessl R and Chapman J N 1995 *Phys. Rev.* B **51** 15964
[23] Yang F, Shang C H, Chien C L, Ambrose T, Krebs J J, Prinz G A, Nikitenko V I, Gornakov V S, Shapiro A J and Shull R D 2002 *Phys. Rev.* B **65** 174410